J Neurophysiol 113: 434–444, 2015.
First published October 29, 2014; doi:10.1152/jn.00539.2014.

Contrast-dependent phase sensitivity in V1 but not V2 of macaque visual cortex

Shaun L. Cloherty[1,2,3] and Michael R. Ibbotson[1,2]

[1]*National Vision Research Institute, Australian College of Optometry, Carlton, Victoria, Australia;* [2]*ARC Centre of Excellence for Integrative Brain Function and Department of Optometry and Vision Sciences, University of Melbourne, Parkville, Victoria, Australia; and* [3]*Department of Electrical and Electronic Engineering, University of Melbourne, Parkville, Victoria, Australia*

Submitted 24 July 2014; accepted in final form 23 October 2014

Cloherty SL, Ibbotson MR. Contrast-dependent phase sensitivity in V1 but not V2 of macaque visual cortex. *J Neurophysiol* 113: 434–444, 2015. First published October 29, 2014; doi:10.1152/jn.00539.2014.— Some neurons in early visual cortex are highly selective for the position of oriented edges in their receptive fields (simple cells), whereas others are largely position insensitive (complex cells). These characteristics are reflected in their sensitivity to the spatial phase of moving sine-wave gratings: simple cell responses oscillate at the fundamental frequency of the stimulus, whereas this is less so for complex cells. In primates, when assessed at high stimulus contrast, simple cells and complex cells are roughly equally represented in the first visual cortical area, V1, whereas in the second visual area, V2, the majority of cells are complex. Recent evidence has shown that phase sensitivity of complex cells is contrast dependent. This has led to speculation that reduced contrast may lead to changes in the spatial structure of receptive fields, perhaps due to changes in how feedforward and recurrent signals interact. Given the substantial interconnections between V1 and V2 and recent evidence for the emergence of unique functional capacity in V2, we assess the relationship between contrast and phase sensitivity in the two brain regions. We show that a substantial proportion of complex cells in macaque V1 exhibit significant increases in phase sensitivity at low contrast, whereas this is rarely observed in V2. Our results support a degree of hierarchical processing from V1 to V2 with the differences possibly relating to the fact that V1 combines both subcortical and cortical input, whereas V2 receives input purely from cortical circuits.

visual system; macaque cortex

IN THE PRIMATE BRAIN, visual information is processed by a network of cortical areas (Felleman and Van Essen 1991). Information from the lateral geniculate nucleus (LGN) enters the cortical network in the primary visual cortex (V1). V1 is reciprocally connected to the second visual area (V2) and other areas in the cortical network. Based on their anatomic connectivity, cortical areas V1 and V2 are often considered sequential stages in a functional hierarchy (e.g., Lund 1988). Whereas V1 receives input from the LGN, V2 receives the majority of its input from V1. However, both areas are modulated by cortical connections. In both primate brain areas, most neurons are selective for the orientation and the spatial and temporal frequency of moving gratings presented within their excitatory receptive fields (Foster et al. 1985), as is also the case in many other mammalian species (e.g., cat: Hubel and Wiesel 1962; rodent: Girman et al. 1999; marsupial: Ibbotson and Mark 2003). Some cortical neurons are selective for the spatial phase of the gratings (simple cells), whereas others (complex cells) are considered phase invariant (Movshon et al. 1978a,b; but also see Hietanen et al. 2013). In addition to their selectivity for visual stimulus attributes, neural responses are modulated by both spatial and temporal stimulus context. Responses to stimuli presented within the excitatory receptive field of a neuron may be modulated by stimuli presented outside of their receptive field (Sengpiel et al. 1997) or by previously presented stimuli (Ohzawa et al. 1982, 1985). Also, selectivity for size and spatial frequency of neurons in V1 is dependent on stimulus contrast (Kapadia et al. 1999; Sceniak et al. 1999, 2002; Shushruth et al. 2009). A proportion of complex cells in primary visual cortex increase their phase sensitivity at low contrast following contrast adaptation and in the presence of stimuli presented within the inhibitory surround of their receptive field (cat: Bardy et al. 2006; Crowder et al. 2007; Romo et al. 2011; van Kleef et al. 2010; monkey: Durand et al. 2012; Henry and Hawken 2013).

Here, for the first time, we investigate the effect of stimulus contrast on the observed phase sensitivity of complex cells in primate area V2 and compare it with V1 using a novel analysis technique that controls for changes in spike count. This affords an informative comparison of two processing stages. Responses in V1 reflect cortically modulated input from the LGN, whereas responses in V2 reflect cortically modulated cortical input. We show that a proportion of complex cells in V1 exhibit increased phase sensitivity at low stimulus contrast. In most cases, this increase is most prominent at threshold contrast, which we defined as the lowest contrast evoking a just-detectable response determined using a receiver operating characteristic (ROC) analysis. By investigating neuronal responses at threshold, we reveal changes in phase sensitivity that emerge at the limits of spatial and temporal summation. Although our data demonstrate dynamic phase sensitivity in a significant proportion of neurons in V1, we find that phase sensitivity of neurons in V2 is largely contrast invariant. This suggests that in primates the cortical networks underlying responses in V2 summate information in a different way from the combined LGN and cortical networks underlying responses in V1.

MATERIALS AND METHODS

Electrophysiology. We made extracellular recordings of spiking responses from 300 well-isolated single units in V1 ($n = 166$) and V2

Address for reprint requests and other correspondence: S. L. Cloherty, National Vision Research Institute, Australian College of Optometry, Cnr Cardigan and Keppel Streets, Carlton, VIC 3053, Australia (e-mail: cloherty@nvri.org.au).

($n = 134$) of 6 anesthetized macaque monkeys (5 *Macaca fascicularis*, 4.3–4.7 kg; 1 *M. nemestrina*, 8 kg). All surgical and experimental procedures were approved by the Animal Welfare Committee at New York University and conformed to the National Institutes of Health *Guide for the Care and Use of Laboratory Animals*. Monkeys were prepared for acute electrophysiological recordings using procedures identical to those described in Cavanaugh et al. (2002). A craniotomy was performed over V1, centered 10 mm posterior to interaural zero and 12 mm lateral to the midline. Extracellular recordings were made with quartz/platinum-tungsten microelectrodes (Thomas Recording), which penetrated the surface of V1 2–4 mm behind the lunate sulcus. Electrodes were advanced in the rostral direction at an angle of 20° from vertical within a parasagittal plane 10–13 mm lateral to the midline. Electrode penetrations traversed the gray matter in V1 followed by a region of white matter (characterized by an absence of spiking activity) before entering the gray matter in V2 on the posterior bank of the lunate sulcus (typically 2,500–3,500 μm from the start of the penetration on the surface of V1). Recorded units were ascribed to either V1 or V2 on the basis of their position relative to the surface of V1, the relationship with the transitions between gray and white matter, and by tracking changes in receptive field topography along the electrode track. Our electrode penetrations were such that cells encountered in V1 and V2 had receptive fields of similar eccentricity; receptive fields for most cells were between 2 and 5° eccentricity. For the purpose of assessing the laminar distribution of recorded cells, the relative cortical depth for each recorded cell was calculated as a fraction of the distance along the electrode track.

Signals from the microelectrodes were amplified, band-pass filtered (300 Hz to 10 kHz), and sampled with 16-bit precision at a rate of 25 kHz. Single units were isolated online using dual-window time-amplitude discrimination software (Expo; P. Lennie, University of Rochester). Spike times were saved with a temporal resolution of 0.1 ms.

Visual stimuli and data acquisition. Visual stimuli were generated by an Apple Macintosh computer running Expo. Stimuli were presented on a calibrated EIZO FlexScan T966 CRT monitor at a resolution of 1,280 × 960 pixels (width × height) and a refresh rate of 120 Hz. The monitor was viewed by the animal from a distance of 114 cm, subtending 20 × 15° of visual angle. The mean luminance of the monitor was 31.2 cd/m^2. Stimuli were presented monocularly on a mean gray background and consisted of luminance-modulated sine-wave gratings windowed by a soft-edged circular aperture centered on the receptive field of the dominant eye. For each cell, we first determined the direction, spatial frequency, temporal frequency, and size of the grating that evoked the maximal response. We then studied the response of each cell to optimal moving sine-wave gratings of 10 different Michelson contrasts equally spaced on a log scale between 0.01 and 1.0. Gratings and a blank (mean gray) condition were presented for 1 s, interleaved in block pseudorandom order, with no interstimulus interval. For each cell, the stimulus was repeated as often as was practical (median 20 times) depending on the stability of the isolation of the cell.

Analysis of neuronal responses. For each cell, we computed the mean firing rate for each stimulus condition, including the blank condition, within an analysis window equal to the stimulus duration (1 s). We chose the onset of the analysis window to maximize the variance of the mean firing rate across all stimulus conditions (Smith et al. 2005). For each trial, we discarded the response to the first cycle of the stimulus to remove the influence of onset transients (Ibbotson and Mark 1996) and then cycle-averaged the responses to each stimulus condition across trials. We estimated the baseline spontaneous activity of each cell as the mean spike count during presentation of the blank condition. At each stimulus contrast, we quantified the phase sensitivity of the cell by Fourier analysis of the cycle-averaged spiking response. Specifically, we calculated the relative modulation, F_1/F_0, of the responses as the amplitude of the Fourier component at the fundamental frequency of the grating stimulus (F_1) divided by the mean response (F_0) after subtraction of the estimated baseline spontaneous activity. We classified cells as simple or complex according to the observed F_1/F_0 at maximum contrast (Dean 1981; Movshon et al. 1978a,b; Skottun et al. 1991).

We compared relative modulation of the observed responses at high and low stimulus contrast. For each cell, the high-contrast condition was defined as the stimulus contrast that evoked the maximal response. For most cells, this was 100% contrast. For 2 cells (1 in each of V1 and V2), the maximal response was observed at 60% contrast. The low-contrast condition was defined as the lowest stimulus contrast tested that evoked a response significantly above the baseline spontaneous rate of the cell. Owing to differences in contrast gain, the low-contrast condition was different for each cell. We determined the appropriate low-contrast condition for each cell based on a ROC analysis (Green and Swets 1966; Tolhurst et al. 1983). Specifically, we compared the observed spike counts for each stimulus contrast tested with those observed during presentation of the blank condition. We quantified the discriminability of the response to each stimulus contrast as the area under the ROC. This represents the probability that an ideal observer would correctly distinguish the grating of a given contrast from the blank stimulus. To assess the significance of the area under the observed ROC at each stimulus contrast, we performed a permutation test (Efron and Tibshirani 1993). We sampled without replacement from the available pool of responses, without regard to the stimulus that was presented (be it the blank or the grating stimulus), and calculated the resulting area under the ROC. This sampling procedure was repeated 10,000 times, producing a null distribution for the area under the ROC. The response to a given stimulus contrast was deemed significantly above the baseline rate if the area under the observed ROC exceeded 99% of the null distribution (i.e., $P < 0.01$).

Expected increase in F_1/F_0 with reduced spike count. Quantifying phase sensitivity by Fourier analysis of spiking responses is sensitive to the number of spikes recorded (Crowder et al. 2007; Hietanen et al. 2013). To account for the increase in F_1/F_0 due to the reduction in the number of spikes as stimulus contrast was reduced, we compared the observed F_1/F_0 of each cell with an empirical distribution of F_1/F_0 derived from a model complex cell. The model cell produces responses containing n spikes over a response interval T, which we define to be one cycle of an optimal sine-wave grating. Spike arrival times, $t_i \in [-\pi, \pi)$, $i = 1 \ldots n$, are assumed to be independent, identically distributed random variables drawn from a raised cosine distribution defined by:

$$f(t;A,B) = \frac{1}{2\pi}\lfloor 1 + A\cos(t-B)\rfloor \quad B-\pi \le t < B+\pi \quad (1)$$

where $0 \le A \le 1$ defines the assumed true or asymptotic F_1/F_0 (i.e., the expected value of F_1/F_0 as $n \to \infty$, denoted as $\langle F_1/F_0\rangle_\infty$) and B defines the position of the distribution. The standard raised cosine distribution corresponds to $A = 1$ and $B = 0$. For $A = 0$, *Eq. 1* reduces to the uniform distribution, corresponding to an ideal phase-invariant complex cell. To simulate responses with a given asymptotic $\langle F_1/F_0\rangle_\infty$, we set $A = \langle F_1/F_0\rangle_\infty$ and $B = 0$.

We determined the appropriate asymptotic F_1/F_0 for each cell by maximizing the likelihood of the data observed. Specifically, for each cell, we computed the log likelihood L of the data for a given asymptotic F_1/F_0 as follows:

$$\log L = \log\textstyle\prod_j f(A_n|A) \quad (2)$$

where A_n is the relative modulation (i.e., F_1/F_0) of the cell based on the observed response containing n spikes, A is the specified asymptotic level of response modulation for the model (*Eq. 1*), and j is an index over stimulus contrast (here indexing the stimulus contrast producing the maximal response).

After choosing the asymptotic F_1/F_0 for the model to maximize the likelihood of the data observed at maximum contrast, we computed

distributions of F_1/F_0 at spike counts (n) corresponding to the number of spikes recorded at each of the lower stimulus contrasts tested for each cell. From these distributions, we calculated 99% confidence limits for the increase in F_1/F_0, which might be expected simply due to the reduction in the number of spikes observed. For the increase in F_1/F_0 observed for a given cell at low contrast to be considered significant, it must exceed the increase in F_1/F_0 expected simply due to the reduction in the number of spikes, i.e., it must exceed the 99% confidence limit of the corresponding empirical distribution.

RESULTS

We made extracellular recordings of spiking responses from neurons in V1 and V2 of six anesthetized monkeys. Specifically, we quantified the phase sensitivity of the response of each cell to optimal moving sine-wave gratings over a range of stimulus contrasts.

Spiking responses from an example complex cell in macaque V1 are shown in Fig. 1*A* for a range of stimulus contrasts. When tested at 100% contrast (Fig. 1*A*, *right*), this cell exhibits a moderate level of response modulation (F_1/F_0 = 0.44). Weak modulation of spiking responses to optimal moving sine-wave gratings is characteristic of many complex cells (Hietanen et al. 2013; Ibbotson et al. 2005). As contrast is reduced (Fig. 1*A*, *middle* and *left* panels), the relative contribution of the modulated component of the response to the overall response of the cell increases. The response of this cell was indistinguishable from the spontaneous background for stimulus contrasts below 8%. Figure 1*B* shows the amplitude of the mean response (F_0) and first harmonic Fourier component (F_1) for this cell plotted against stimulus contrast. The mean component of the response decreases monotonically with decreasing stimulus contrast, whereas the modulated response component (F_1) peaks at moderate stimulus contrast (36%). Despite the reduction in overall response amplitude, the relative modulation (F_1/F_0) of the response increases monotonically with decreasing stimulus contrast (Fig. 1*C*).

Fourier analysis of spiking responses is sensitive to the number of spikes observed: F_1/F_0 is expected to increase as the number of spikes observed is reduced (Hietanen et al. 2013). Any increase in F_1/F_0 as contrast is reduced is therefore confounded by the concomitant reduction in the number of spikes. In assessing the magnitude of any observed change in F_1/F_0, it is therefore necessary to control for the effect of changes in spike count. Figure 2 illustrates the relationship between expected F_1/F_0 and spike count derived from the model complex cell for a range of asymptotic F_1/F_0 values (red curves; the asymptotic F_1/F_0 value giving rise to each curve is indicated in red on the right of Fig. 2*A*). For low spike counts, the expected value of F_1/F_0, denoted by $\langle F_1/F_0 \rangle$, may lie far from the specified asymptotic F_1/F_0 value. The exact value of $\langle F_1/F_0 \rangle$ depends on the number of spikes (n). As n approaches the lower bound of 1 spike, $\langle F_1/F_0 \rangle$ approaches 2 (all of the curves in Fig. 2*A* converge to $F_1/F_0 = 2$ at $n = 1$).

Consider again the example cell shown in Fig. 1. For this cell, we recorded a total of 1,130 spikes across all repeats at a stimulus contrast of 100% and estimated $F_1/F_0 = 0.44$ (Fig. 1*C*). Figure 2*B* shows the likelihood of the observed data as a function of the assumed asymptotic F_1/F_0 value (leftmost curve). The likelihood peaks at $F_1/F_0 = 0.44$. This is consistent with the value estimated from the data, as expected given the relatively large number of spikes recorded for this cell at 100% contrast and the shallow slope of the relationships illustrated in Fig. 2*A*. The relationship between $\langle F_1/F_0 \rangle$ and spike count for an asymptotic $F_1/F_0 = 0.44$ is shown by the thick red line in Fig. 2*A*. Figure 2*C* shows empirical distributions of F_1/F_0 for 50, 100, and 500 spikes for the model complex cell with an asymptotic $F_1/F_0 = 0.44$. As the number of spikes increases, the mean of the empirical distribution (i.e., $\langle F_1/F_0 \rangle$, indicated by the solid red lines in Fig. 2*C*) approaches the specified asymptotic F_1/F_0 value and the spread of the distribution decreases (broken lines indicate the 99% confidence limit for each distribution).

For comparison of the model with the experimental data from the example cell, Fig. 2*A* shows the observed F_1/F_0 for the example cell for stimulus contrasts between 8 and 100%

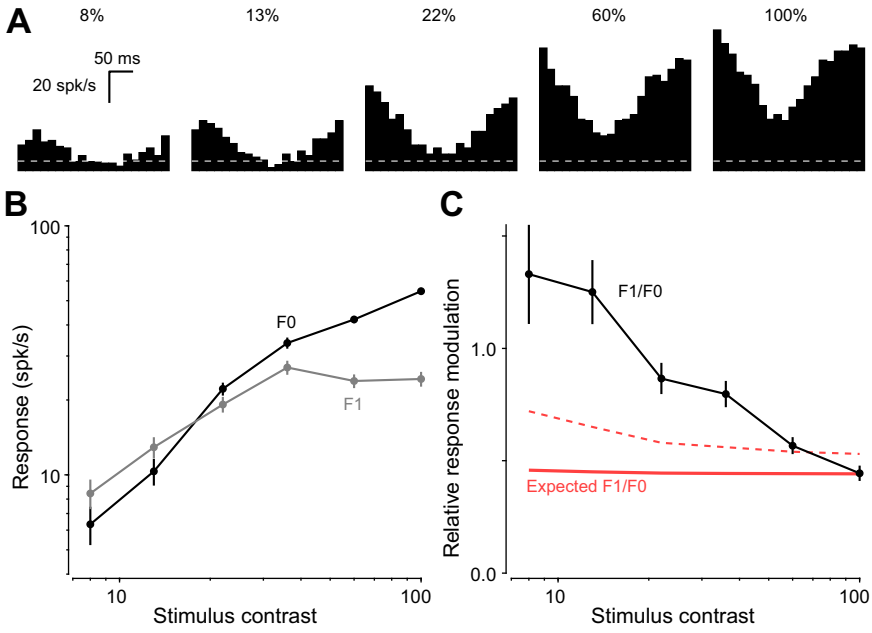

Fig. 1. Relative modulation of spiking responses from a V1 complex cell. The stimulus was an optimal moving sine-wave grating with contrast ranging from 8 to 100%. *A*: cycle histograms for responses observed for stimulus contrasts of 8, 13, 22, 60, and 100% (*left* to *right*). The dashed line indicates the baseline spontaneous rate. *B*: amplitude of the mean (F_0) and modulated (F_1) components of the response of the cell as functions of stimulus contrast. Stimulus contrasts <8% failed to elicit a discernable response (data not shown). *C*: relative modulation of the response of the cell, i.e., F_1/F_0, as a function of stimulus contrast (black). The solid red line indicates the expected F_1/F_0 for a model complex cell fitted to the data at 100% contrast (asymptotic F_1/F_0 = 0.44). The model assumes the underlying phase sensitivity of the cell is contrast invariant, and any change in relative modulation of responses, as contrast is reduced, is due to a reduction in the observed spike counts. The model provides an empirical distribution for F_1/F_0, accounting for the number of spikes observed at each stimulus contrast. The broken red line indicates the 99% confidence limit for the expected F_1/F_0 derived from these empirical distributions. At low contrast, the model complex cell provides a poor account of the observed data. In *B* and *C*, symbols indicate the mean (cycle-averaged) amplitude of the respective response metric, and error bars show bootstrap estimates of the standard error. spk/s, Spikes per second.

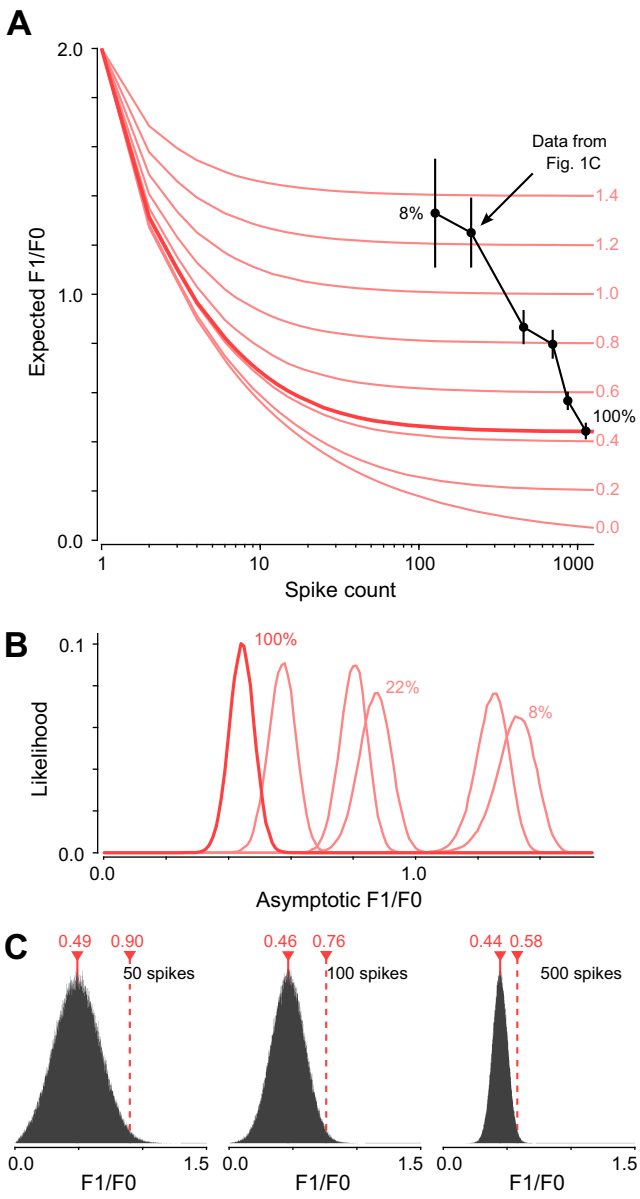

Fig. 2. Modeling the effect of observed spike count on the expected F_1/F_0. *A*: red curves show the relationship between expected F_1/F_0 and spike count, derived from empirical distributions of F_1/F_0 for a range of assumed asymptotic F_1/F_0 values (see MATERIALS AND METHODS). Asymptotic F_1/F_0 for each curve is indicated on the right. The thick red line shows the expected F_1/F_0 for a model complex cell fitted to the responses of the example cell shown in Fig. 1 (asymptotic $F_1/F_0 = 0.44$). Black symbols show observed F_1/F_0 for the example cell at each stimulus contrast plotted against the corresponding number of spikes recorded. Clearly, the model (thick red line) fails to account for the increase in F_1/F_0 observed at low stimulus contrast. *B*: likelihood of the observed F_1/F_0 for the example cell at each stimulus contrast as functions of the asymptotic F_1/F_0 of the model. These curves peak at progressively greater asymptotic F_1/F_0 values as contrast is reduced, revealing the failure of the model (i.e., a single asymptotic F_1/F_0 value) to account for the increase in observed F_1/F_0 as contrast is reduced and indicating a change in the neuronal mechanism underlying responses at high and low contrast. *C*: empirical distributions of simulated F_1/F_0 for the model complex cell ($F_1/F_0 = 0.44$) for 50, 100, and 500 spikes (*left* to *right*). In each case, the expected value of the distribution is indicated by the solid red line, and the corresponding 99% confidence limit is indicated by the broken red line. These distributions illustrate the increased bias and uncertainty of estimating F_1/F_0 as spike count is reduced.

(black symbols). These are the same data points as shown in Fig. 1*C*, plotted against their corresponding spike counts. For further comparison of the model with the observed data, $\langle F_1/F_0 \rangle$ for the complex cell model is also plotted against stimulus contrast in Fig. 1*C* (solid red line) together with the corresponding 99% confidence limits (broken red line). Clearly, Figs. 1 and 2 illustrate that for the example cell the increase in F_1/F_0 observed as stimulus contrast is reduced far exceeds that expected due to the reduction in spike count alone. For even moderate stimulus contrasts, the observed F_1/F_0 lies well above the 99% confidence limit (Fig. 1*C*). Figure 2*B* also shows the likelihood of the data observed at each stimulus contrast (and corresponding spike count) as functions of the assumed asymptotic F_1/F_0 value. The peaks of these curves move to the right as contrast is reduced. This shift reveals the failure of a static model (i.e., a single asymptotic F_1/F_0) to explain the level of relative modulation observed at all stimulus contrasts, suggesting a change in the operating regime (i.e., the asymptotic F_1/F_0) of the cell as contrast is reduced.

To quantify the change in F_1/F_0 with contrast across our cell populations in V1 and V2, we compared the F_1/F_0 observed at high contrast with that observed at threshold contrast for each cell. Owing to differences in contrast gain between cells, the low-contrast condition was necessarily different for each cell. We determined the appropriate low-contrast condition (i.e., threshold contrast) for each cell based on a ROC analysis. Figure 3*A* shows ROCs for the example cell corresponding to each of the stimulus contrasts tested. Spiking responses of this cell were not significantly different from the spontaneous background for stimulus contrasts below 8% (permutation test, $P > 0.01$; ROCs shown in gray). Figure 3, *B* and *C*, shows the distribution of threshold contrast for cells in V1 and V2, respectively (colored bars, complex cells; gray bars, simple cells). Both of these distributions deviate from normal (Lilliefors' goodness-of-fit test, $P > 0.05$). We found no significant difference between these 2 distributions (2-sample Kolmogorov-Smirnov goodness-of-fit test, $P = 0.78$). Figure 3, *D* and *E*, shows corresponding distributions of the area under the ROCs for all cells in V1 and V2, respectively. Comparison of the distributions in Fig. 3, *B*–*E*, reveals no systematic difference between the stimuli or the detectability of responses used to assess phase sensitivity in V1 and V2.

Figure 4*A* shows F_1/F_0 at the lowest contrast that produced a significant response (based on the ROC analysis) plotted against F_1/F_0 at high contrast for 166 cells from V1. The median F_1/F_0 for our complex cell population in V1 increased from 0.33 at high contrast to 0.65 at threshold contrasts. Individually, 46/105 (44%) of the complex cells we recorded in V1 exhibited a significant increase in F_1/F_0, i.e., an increase that exceeds their corresponding 99% confidence limit and cannot be attributed simply to a reduction in the number of spikes observed. These cells are indicated by the green symbols in Fig. 4*A*. Figure 4*B* shows comparable data for 134 cells from V2. We observed a much smaller increase in median F_1/F_0 for complex cells in V2 as contrast was reduced (0.33 at threshold contrasts compared with 0.29 at high contrast). Notably, the number of complex cells for which the observed increase in F_1/F_0 could not be attributed to a reduction in the number of spikes observed was very small in V2 (9/122 cells, 7%; blue symbols in Fig. 4*B*).

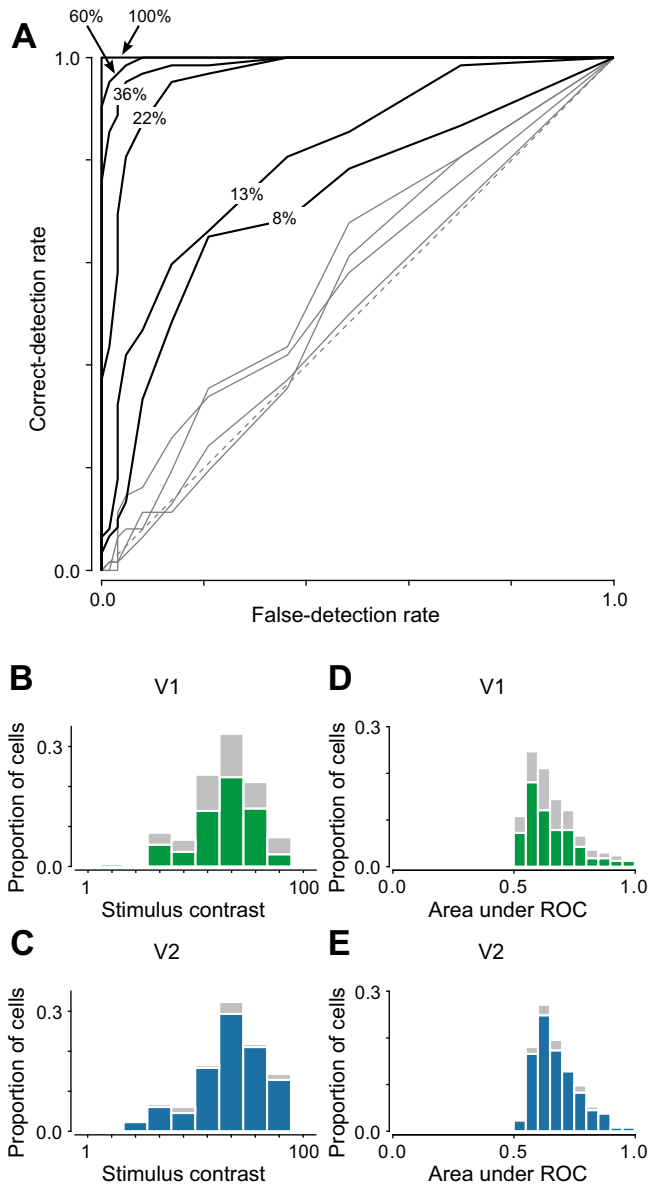

Fig. 3. Definition of threshold contrast. *A*: receiver operating characteristics (ROCs) for the example cell shown in Fig. 1. For this cell, stimulus contrasts below 8% failed to elicit responses demonstrably different from the background spontaneous rate (gray curves). For stimulus contrasts of 8% and above, responses were significantly greater than the background spontaneous rate ($P < 0.01$, permutation test; black curves). *B* and *C*: distributions of the lowest stimulus contrast that evoked a significant response (based on the ROC analysis) for all cells in V1 and V2, respectively. Colored bars show the distributions for complex cells, whereas gray bars show the distributions for simple cells. *D* and *E*: distributions of the area under the ROC at threshold contrast for all cells in V1 and V2, respectively (same conventions as in *B* and *C*).

We quantified the change in F_1/F_0 on a cell-by-cell basis for all cells in V1 and V2. Simple cells in both V1 and V2 showed no consistent change in F_1/F_0 with contrast (V1: 0.03, 2-sided Wilcoxon signed-rank test, $P = 0.37$; V2: −0.15, 2-sided Wilcoxon signed-rank test, $P = 0.13$). The situation was very different for complex cells. Figure 4, *C* and *D*, shows distributions of the change in F_1/F_0 at threshold contrast compared with high contrast for complex cells in V1 and V2, respectively. The differences in these distributions are very clear. Complex cells in V1 showed a significant increase in F_1/F_0 at threshold contrasts with a median change across all complex cells in V1 of 0.32 (2-sided Wilcoxon signed-rank test, $P < 0.001$; Fig. 4*C*). In contrast, complex cells in V2 showed a much smaller increase in F_1/F_0 at threshold contrasts (median change 0.08; 2-sided Wilcoxon signed-rank test, $P < 0.001$; Fig. 4*D*). When assessed individually, a subset of complex cells in both V1 and V2 exhibited a significant increase in F_1/F_0 at threshold contrast (colored symbols in Fig. 4, *A* and *B*). The distributions of the change in F_1/F_0 for those cells is shown by the colored bars in Fig. 4, *C* and *D*. Among those cells, the magnitude of the change was comparable in V1 and V2 (median increase of 0.64 and 0.57, respectively; Wilcoxon rank-sum test, $P = 0.92$). However, as already noted, the proportion of complex cells in V2 exhibiting a significant increase in F_1/F_0 at threshold contrast was very low (only 7% for V2 vs. 44% for V1).

Although the distributions of the change in F_1/F_0 for complex cells in V1 and V2 (Fig. 4, *C* and *D*) show the absolute change in relative modulation of observed responses, this difference does not account for the influence of reduced spike count at low contrast. For each cell, we quantified the change in F_1/F_0 not attributable to a reduction in spike count by subtracting $\langle F_1/F_0 \rangle$ given by the model from F_1/F_0 observed at threshold contrast. If the F_1/F_0 ratio observed at threshold contrast was due to limited spike count, we would expect this difference to be distributed around 0. The distributions of this metric for complex cells in V1 and V2 are shown in Fig. 4, *E* and *F*, respectively. Across all complex cells in V1, this metric was significantly greater than 0 (median 0.24; 2-sided Wilcoxon signed-rank test, $P < 0.001$; Fig. 4*E*). This reveals that on average, complex cells in V1 show greater relative modulation of their responses at low contrast than would be expected due to reduced spike count. This is not the case in V2. The median of the distribution for V2 is not significantly different from 0 (median −0.005, 2-sided Wilcoxon signed-rank test, $P = 0.99$; Fig. 4*F*), suggesting that in V2 the relative modulation of responses at low contrast is adequately explained by the reduced spike count.

The colored bars in Fig. 4, *E* and *F*, show the distributions for the subset of complex cells in V1 and V2 that showed a significant increase in F_1/F_0 when assessed individually. The medians of the distributions for V1 and V2 are comparable (V1, 0.53; V2, 0.52; Wilcoxon rank-sum test, $P = 0.99$) and significantly greater than 0 (V1, $P < 0.001$; V2, $P = 0.003$; Wilcoxon signed-rank test).

To allow comparison of the absolute response rate for our cells recorded in V1 and V2, Fig. 5 shows distributions of the F_0 and F_1 response components recorded at maximum contrast for all cells. Figure 5, *A* and *B*, shows the distributions of F_0 and F_1, respectively, for cells recorded in V1, whereas Fig. 5, *C* and *D*, shows comparable distributions for cells recorded in V2 (colored bars, complex cells; gray bars, simple cells). For the majority of complex cells in both V1 and V2, the F_0 response component had amplitudes between 0 and 70 spikes per second. A small proportion of complex cells in V1 had F_0 amplitudes >70 spikes per second. In both V1 and V2, the F_1 response components had amplitudes between 0 and 30 spikes per second. Altogether, our populations of complex cells recorded in V1 and V2 generated responses with comparable overall spike rates, and it is unlikely that the small differences

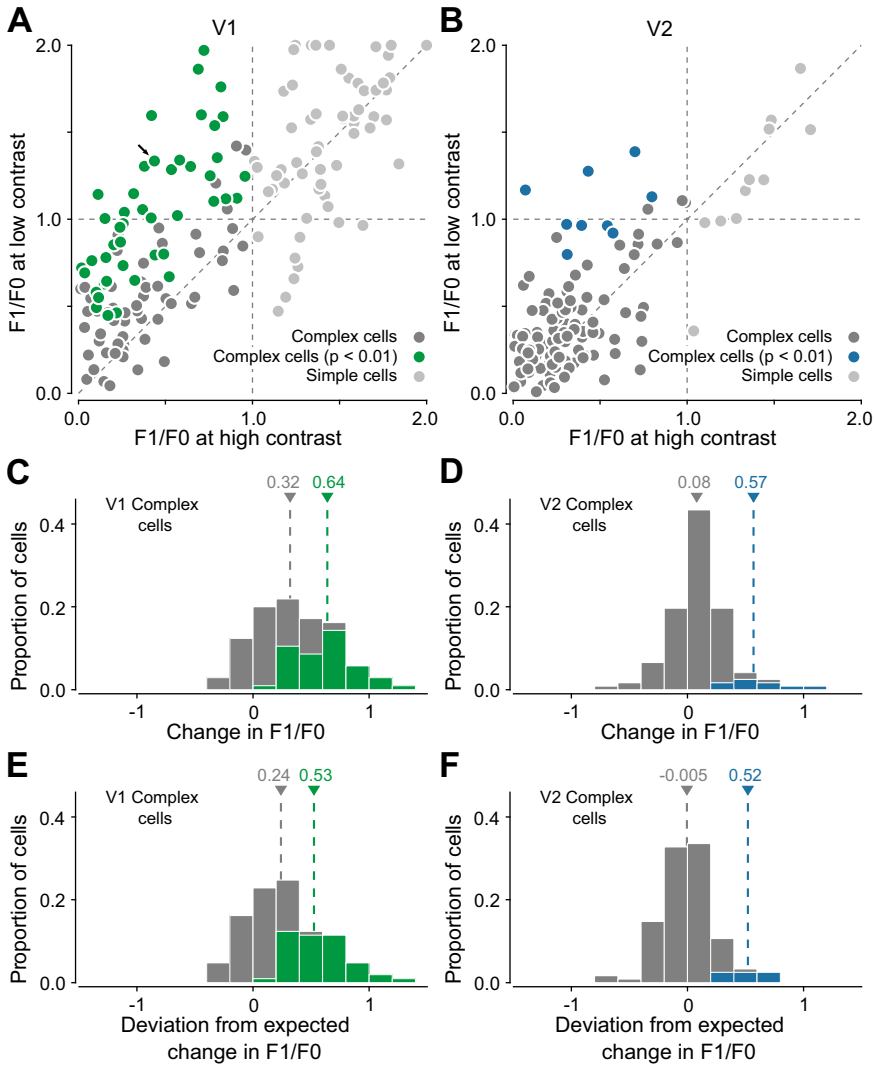

Fig. 4. Relative modulation (F_1/F_0) of responses at low compared with high stimulus contrast. *A*: scatterplot of F_1/F_0 observed at threshold contrast plotted against F_1/F_0 observed at high contrast for 166 cells in V1. Each symbol represents a single cell. *B*: similar data for 134 cells in V2. In *A* and *B*, complex cells exhibiting a significant ($P < 0.01$) increase in F_1/F_0 at threshold contrast are shown in green (V1) and blue (V2), respectively. The remaining complex cells are indicated by the dark gray symbols. Simple cells are shown by the light gray symbols. The example cell shown in Fig. 1 is indicated by the arrow (black) in *A*. *C* and *D*: histograms of the change in F_1/F_0 at threshold contrast compared with that at high contrast for complex cells in V1 and V2, respectively. Colored bars show the distributions for the subset of complex cells showing a significant increase in F_1/F_0. The median change in F_1/F_0 for each distribution is indicated by the broken line. *E* and *F*: distributions of relative modulation of responses observed at threshold contrast for complex cells in V1 and V2, respectively, after accounting for the effect of reduced spike count. Complex cells in V1 (*E*) show significantly greater relative modulation of their responses at threshold contrasts than is expected due to reduced spike count (median 0.24; 2-sided Wilcoxon signed-rank test, $P < 0.001$). In contrast, the median of the distribution for complex cells in V2 is not significantly different from 0 (median −0.005; 2-sided Wilcoxon signed-rank test, $P = 0.99$), demonstrating that relative modulation of responses of complex cells in V2 (*F*) is consistent with that expected due to reduced spike count.

in absolute response rate could account for the dramatic difference we observe between the 2 cell populations.

Laminar organization. To investigate the laminar distribution of our cells, Fig. 6, *A* and *B*, shows the relative cortical depth for all recorded cells in V1 and V2, respectively, plotted against the relative modulation of their responses at high contrast. In each case, the running median F_1/F_0 computed with a window size of 100 μm is shown superimposed (solid black line). For our population of cells from V1 (Fig. 6*A*), the running median F_1/F_0 exhibits a characteristic pattern of peaks and troughs that correlates well with that previously reported for macaque V1 (Ringach et al. 2002; shown by the dashed black line in Fig. 6*A*). The correlation between the running median F_1/F_0 for our data and that reported by Ringach et al. (2002) is extremely high ($r = 0.795$, $P < 0.001$). Green symbols in Fig. 6*A* indicate those complex cells that exhibit a significant increase in relative modulation of their responses at threshold contrast. These cells were found in all cortical layers.

Figure 6*C* shows the change in F_1/F_0 not attributable to a reduction in observed spike count for all complex cells recorded in V1. This is the same metric as shown in Fig. 4*E*, plotted here at the relative cortical depth for each cell. The running median, computed with a window size of 100 μm, is shown superimposed (solid black line). To identify regions in which the median change in F_1/F_0 is greater than expected due to a reduction in observed spike count, we performed a bootstrap hypothesis test (Efron and Tibshirani 1993). Specifically, we sampled with replacement from the total pool of complex cells recorded in V1 and computed the running median of the change in F_1/F_0 not attributable to a reduction in spike count. This sampling procedure was repeated 10,000 times to obtain a distribution, at each cortical depth, of the median change in F_1/F_0 not attributable to a reduction in spike count. At each cortical depth, the observed median change in F_1/F_0 was deemed to be significant only if the proportion of samples for which the median change was <0 was <0.05. Gray bars in Fig. 6*C* indicate those regions in which the median change in F_1/F_0 is significantly greater than 0 (i.e., $P < 0.05$). This criterion is satisfied at most cortical depths.

In V2, the running median F_1/F_0 was below unity at all cortical depths (Fig. 6*B*). The 11 simple cells that we recorded in V2 were located at relative cortical depths between 0.2 and 0.8 (Fig. 6*B*). This is consistent with previous reports suggesting that simple cells are located most frequently in the upper and middle layers of V2 (Levitt et al. 1994).

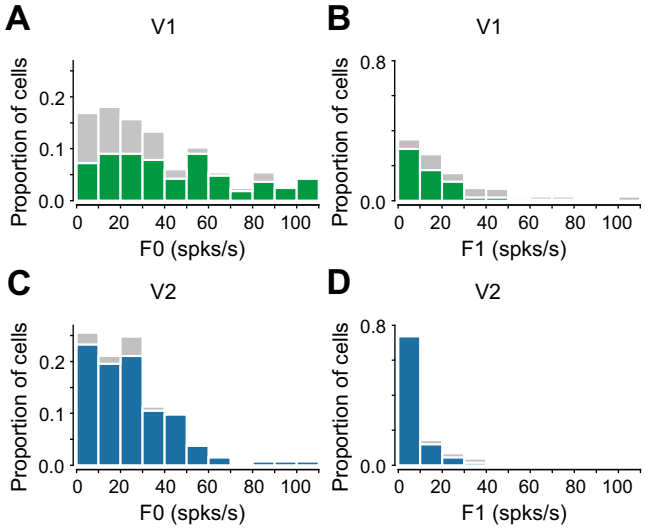

Fig. 5. Distribution of F_0 and F_1 in V1 and V2. *A* and *B*: distributions of F_0 and F_1, respectively, for all cells recorded in V1. *C* and *D*: comparable distributions of F_0 and F_1 for all cells recorded in V2. In all cases, colored bars show the distributions for complex cells, whereas gray bars show the distributions for simple cells.

Figure 6*D* shows the change in F_1/F_0 not attributable to a reduction in observed spike count for all complex cells recorded in V2. In contrast to V1 (Fig. 6*C*), the median change in F_1/F_0 in V2 was not significantly different from 0 at any cortical depth (bootstrap, $P > 0.05$). Nevertheless, of the 9 complex cells in V2 that exhibit a significant increase in relative modulation of their responses at threshold contrast (blue symbols in Fig. 6*B*), most were located in the lower and middle layers. The interquartile range (IQR) of their relative cortical depths was 0.57–0.72 (nominally corresponding to layers 4 and 5). To assess whether this apparent clustering is greater than expected, we compared this IQR with the distribution of IQRs expected by chance. Specifically, we randomly sampled 9 cells, with replacement, from the total population of complex cells we recorded in V2 and computed the IQR of their relative cortical depths. This sampling procedure was repeated 10,000 times to produce a distribution of IQRs. The proportion of samples for which the IQR was less than that observed for our data was 0.026, suggesting that the apparent clustering we observed in V2 is unlikely to have arisen by chance.

DISCUSSION

Investigations of neuronal responses in geniculorecipient regions of cat primary visual cortex have shown that reducing stimulus contrast leads to significant increases in the relative modulation (F_1/F_0) of responses to moving gratings among complex cells but not simple cells (Crowder et al. 2007). However, calculating the relative modulation of spiking responses is problematic at low contrast due to the low spike rates encountered: relative modulation increases purely as a result of the reduction in spike count (Hietanen et al. 2013; van Kleef et al. 2010). Therefore, Crowder and colleagues (2007) performed simulations to establish statistical bounds outside which any observed modulation of the spiking responses could not be ascribed solely to low spike count. The observed changes in relative modulation at low contrast for many cells fell outside of these bounds and were, therefore, likely to have arisen from physiological mechanisms. The conclusion was that in many complex cells in cat primary visual cortex, relative modulation of responses increases at low contrast, reflecting a change in the phase sensitivity of the cells.

Henry and Hawken (2013) conducted similar experiments in macaque V1. For each cell, they established a threshold contrast as the lowest contrast for which the mean firing rate exceeded the baseline spontaneous rate ($P > 0.05$). They calculated the relative modulation (F_1/F_0) of cycle-averaged responses at threshold and at twice threshold contrast. They found that 32% of complex cells showed a significant increase in relative modulation of their responses at threshold contrast. This proportion reduced to 17% when assessing responses at twice threshold. Henry and Hawken (2013) concluded that although on average complex cells in their population exhibit an increase in relative modulation of their response at threshold contrast, this was largely a consequence of low firing rates and the finite data available. Although this is true for the majority of their cell population, it is not true for almost a third of cells (32%), which they report exhibited a significant increase in F_1/F_0 at threshold contrast, even after specifically accounting for the effect of reduced spike count. In our recordings, we assessed the responses of V1 and V2 neurons at just-detectable stimulus contrasts. At these contrasts, we found that an even higher proportion (44%) of complex cells in V1 showed a significant increase in relative modulation of their responses. However, the results from V2 were drastically different. Only 7% of complex cells in V2 showed a significant increase in relative modulation of their responses even at just-detectable stimulus contrasts. Our results reveal interesting changes in the summation properties of cortical neurons at just-detectable contrasts. In our view, it seems likely that the observed effects are a consequence of the mechanism by which complex cell receptive fields are formed. If this is the case, it is apparent that the formation of complex cell receptive fields is different in V1 and V2.

Laminar organization. In V1, the axons from the dorsal LGN terminate primarily in layer 4C (Lund 1988). Some LGN axons also provide input to layer 6 (Fitzpatrick et al. 1985; Hendrickson et al. 1978). Most other layers receive minor direct input from the LGN with two exceptions: layers 4B and 5 receive no direct thalamic input (Fitzpatrick et al. 1985; Lund 1988).

The laminar organization of V1 is reflected in the receptive field and response properties of V1 neurons (Gilbert 1977). Notably, simple and complex cells are nonuniformly distributed with respect to cortical layer. Ringach et al. (2002) showed that the median modulation ratio (F_1/F_0) for a large sample of V1 neurons peaked at ~1.4 in the middle of layer 4C (Fig. 6*A*), reflecting a predominance of simple cells in this geniculorecipient layer. They also reported an almost equal distribution of simple and complex cells in layer 6 such that the median F_1/F_0 there was close to unity. These findings demonstrate that simple cells and complex cells exhibiting substantial relative modulation of their responses tend to reside in close proximity to the termination zones of the dominant geniculate inputs. Conversely, the median F_1/F_0 was reportedly well below unity in all other layers (Ringach et al. 2002). Before assessing the laminar distribution of cells in our data set, we

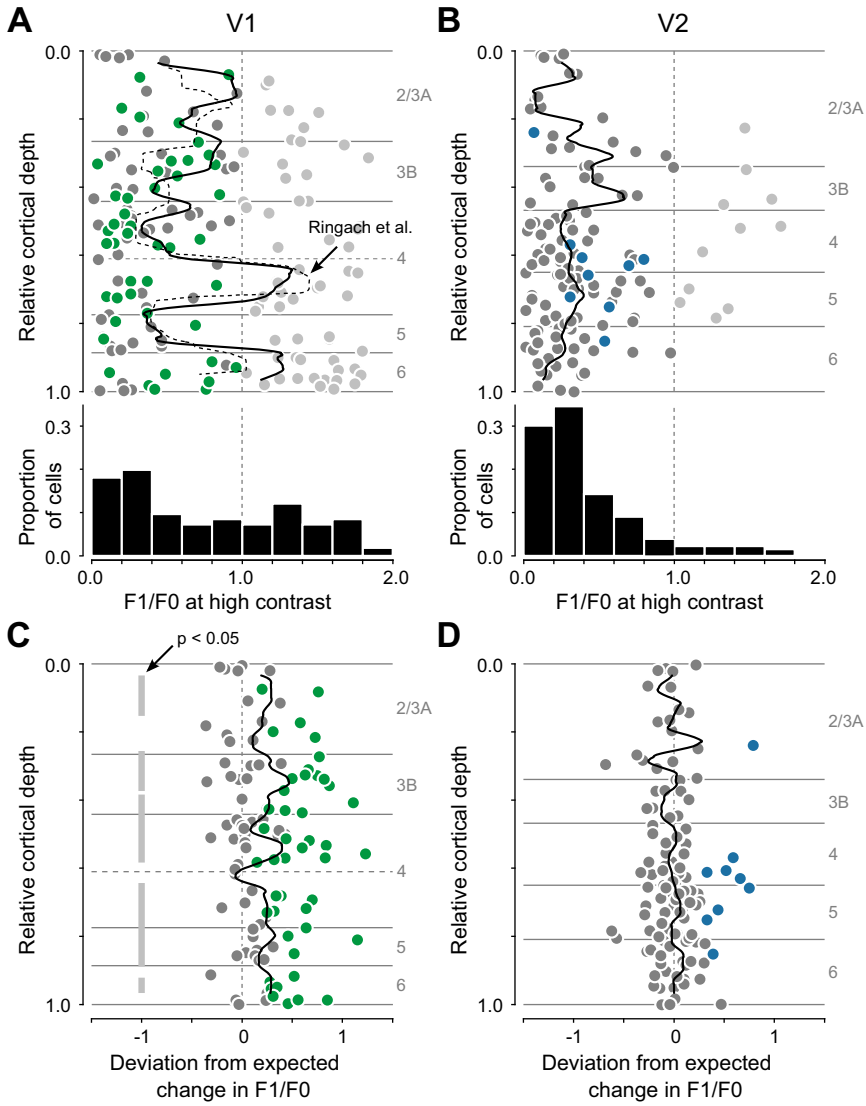

Fig. 6. Laminar distribution of recorded cells. *A*: plot of relative modulation (F_1/F_0) observed at high contrast against relative cortical depth for all cells recorded in V1. Each symbol represents a single cell (same conventions as in Fig. 4*A*). The solid black line shows the running median F_1/F_0 computed with a window size of 100 μm. For comparison, the running median F_1/F_0 from Ringach et al. (2002) is shown by the dashed black line. *B*: plot of relative modulation observed at high contrast against relative cortical depth for all cells recorded in V2 (same conventions as in Fig. 4*B*). Nominal layer boundaries were drawn based on previously published normative measurements of Nissl-stained sections of macaque cortex (V1, Ringach et al. 2002; V2, Lund et al. 1981). The *bottom* of *A* and *B* shows the distributions of F_1/F_0 for all cells recorded in V1 and V2, respectively. *C* and *D*: plots of the change in relative modulation of responses observed at threshold contrast for complex cells in V1 and V2, respectively, after accounting for the effect of reduced spike count. Complex cells in V1 (*C*) show significantly greater relative modulation of their responses at threshold contrasts than is expected due to reduced spike count in all cortical layers (bootstrap, $P < 0.05$). In contrast, for complex cells in V2 (*D*), the median change in F_1/F_0, after accounting for the effect of reduced spike count, is not significantly different from 0 at any cortical depth (bootstrap, $P > 0.05$).

compared the laminar distribution of median F_1/F_0 for our data set against that of Ringach et al. (2002): the two data sets are remarkably similar ($r = 0.795$, $P < 0.001$; for comparison, the median F_1/F_0 from Ringach et al. 2002 is plotted along with our data in Fig. 6*A*). The agreement between our data and those reported previously gives us confidence in the distribution of the cells in our data set.

As noted above, we found complex cells that increase their phase sensitivity at threshold contrast in all cortical layers in V1. Moreover, the median change in relative modulation was significantly greater than expected in all cortical layers. Henry and Hawken (2013) also investigated the laminar distribution of contrast-dependent phase sensitivity in macaque V1. Although they reported an overrepresentation of contrast-dependent phase sensitivity among complex cells in layer 4C and 6, they, too, found cells of this type in all layers.

Afferent connections to V2 from V1 terminate primarily in layers 3B and 4 with less dense terminals also found in layer 3A and the boundary between layers 5 and 6 (Lund et al. 1981). We found very few complex cells in V2 that exhibited significant increases in their phase sensitivity at low contrast. Nevertheless, in contrast to V1, where such cells were found in all layers, those cells we did find in V2 were seemingly clustered in the mid- to lower layers. This apparent clustering is unlikely to have arisen by chance (bootstrap, $P = 0.025$). We therefore tentatively suggest that in area V2 those few complex cells that exhibit a significant increase in phase sensitivity at low contrast are found in layers that receive afferent input from V1 (putatively layers 4 and 5).

Mechanisms. Hubel and Wiesel (1962) proposed a hierarchical model for the formation of cortical receptive fields in which V1 simple cells combine input from the geniculate, engendering them with tuning for orientation and spatial frequency, and V1 complex cells combine input from spatially offset simple cells to generate phase-invariant responses. The laminar organization of area V1, as described in the previous section, lends some qualitative support to a hierarchical model for cortical processing. If some of the geniculate or simple cell inputs to complex cells in layers 3B, 4B, 4C, and 6 have high contrast thresholds, whereas others have low contrast thresholds, reducing contrast to just-detectable levels would greatly reduce the influence of those inputs with high contrast thresholds. As proposed and modeled previously (Crowder et al. 2007; van Kleef et al. 2010), if this were the case, the complex

cells would become more phase sensitive as contrast is reduced.

A similar hierarchical circuit to that proposed to link simple and complex cells in V1 has also been described for connections between cortical areas V1 and V2 (El-Shamayleh et al. 2013). From 59 neurons shown to provide direct input from V1 to V2, ~60% were strongly phase sensitive (i.e., simple). This suggests that complex cells in V2 receive input from a high proportion of V1 simple cells in addition to complex cells, challenging the notion that V1 input to V2 is dominated by complex like spatiotemporal filters (El-Shamayleh et al. 2013). In light of this, it would appear that the V1 input to V2 is similar to the input to complex cells within V1, i.e., a combination of both simple and complex like filters. Despite this similarity in their input, neurons in V2 are thought to combine input from V1 to generate sophisticated feature selectivity not encoded in V1 (Freeman et al. 2013). On this basis, complex cells in V2 are not simply functional replicas of complex cells in V1. Similarly, our results demonstrate that phase sensitivity of complex cells in V2 differs substantially from that in V1. Whereas a substantial proportion of complex cells in V1 exhibit evidence of underlying phase sensitive input when driven near threshold, the same is very rare in V2. It would appear that the mechanisms by which complex cells in V2 combine inputs from simple cells in V1 eliminate the phase sensitivity of those inputs such that it cannot be revealed by simple stimulus manipulations such as reducing contrast. This suggests that distinctly different neural mechanisms for phase averaging and summation are at work for complex cells in V1 and V2.

Although an elegant concept, the hierarchical model is based entirely on feedforward connections, and there is sufficient diversity in V1 complex cell responses that one model cannot explain all effects (Henry 1977; Spitzer and Hochstein 1988). Driven by evidence showing enormous intracortical connectivity (Peters et al. 1994), computational models suggest that simple and complex receptive fields can be created by adjusting the strength of recurrent intracortical connections (e.g., Chance et al. 1999; Tao et al. 2004; Wielaard et al. 2001; Zhu et al. 2009). Such models also overcome problems associated with schemes based only on feedforward connections. For example, the existence of largely linear simple cell receptive fields is difficult to explain based on feedforward connections because of the nonlinearities inherent in their geniculate inputs. However, phase averaging and strong nonlinear inhibition via intracortical connections can effectively "linearize" simple cell responses in recurrent models of cortex (Wielaard et al. 2001). Given that our results show that some complex cell receptive fields in V1 become more linear at low contrast, we suggest that contrast-dependent changes in intracortical connectivity could, at least in part, explain our findings.

The presence of many complex cells in V1 that do not show significant changes in phase sensitivity suggests that the feedforward convergence of simple cells onto complex cells is likely only one mechanism realized in V1. Indeed, many others have been proposed (for review, see Priebe and Ferster 2012), and there is experimental evidence for a diversity of mechanisms: inactivation of layer A in the LGN deactivates layer 4 simple cells but not all layer 2/3 complex cells (Malpeli 1983; Martinez and Alonso 2001; see also Calloway 2001), some complex cells have been shown to receive direct LGN input (Bullier and Henry 1979; Heggelund 1981; Martin and Whitteridge 1984), and many simple cells may receive excitatory input from complex cells (Rust et al. 2005). Based on our experiments, we cannot suggest a single model to explain how or why relative modulation of complex cell responses increases at low stimulus contrast in V1. However, our observations reveal that significant changes do occur, warranting further investigation (for an extensive discussion of possible models, see van Kleef et al. 2010). The fact that V2 shows little change in phase sensitivity suggests that its strictly intracortical connections and increased spatial summation negate any contrast-dependent changes otherwise inherited from V1.

Simple cells in V1 have spatially segregated subregions within their receptive fields that are sensitive to luminance increments (bright subregions) or decrements (dark subregions). For complex cells in V1, this spatial segregation is either less obvious or absent (Hubel and Wiesel 1962; Mata and Ringach 2005). It is possible that the increase in response modulation observed in V1 and V2 complex cells at low stimulus contrast reflects a change in the spatial structure of the receptive fields of the cells. Two studies of receptive fields in macaque cortex support this hypothesis. Using reverse correlation of responses to dynamic noise stimuli, Mata and Ringach (2005) quantified the degree of overlap between bright and dark subregions within the receptive fields and compared the degree of subregion overlap with the observed relative modulation of responses to moving gratings. They showed that measures of subregion overlap are significantly correlated with the relative modulation of responses to moving gratings. Importantly, they also showed that small changes in the relative gain of the bright and dark subregions of the receptive fields can lead to reclassification of cells from simple to complex. These findings suggest that the increase in relative modulation we observe at threshold contrasts could reflect a change in the spatial structure of the receptive fields: either a reduction in subregion overlap or a change in the relative gain of the bright and dark subregions.

Durand et al. (2012) conducted experiments in primate V1 to investigate how the spatial receptive field properties of neurons change as contrast is reduced. They found that there were small but significant reductions in receptive field subregion overlap as contrast was reduced from high to medium values. Although the reduction in overlap was small (no complex cells were reclassified as simple), the finding offers some support for a mechanism in which the increase in phase sensitivity observed by us at lower contrasts may be related to changes in the spatial structure of receptive fields. However, differences in methodology need to be considered carefully. Using stimuli consisting of briefly presented oriented bars, Durand et al. (2012) also noted that receptive field width was decreased significantly as contrast was reduced. However, when using moving gratings, they found that receptive field area increased as contrast was reduced (the latter being consistent with a previous report by Sceniak et al. 1999). Clearly, the way that stimulus contrast influences receptive field structure is somewhat dependent on other stimulus properties. In our experiment, we used optimal moving gratings. Therefore, direct comparison with the observations of Durand et al. (2012) and any interpretation regarding possible mechanisms may not be appropriate.

ACKNOWLEDGMENTS

We thank Prof. J. A. Movshon (Center for Neural Science, New York University), in whose laboratory the recordings were performed. We also thank Drs. Luke Hallum and Adam Morris, who provided comments on the draft manuscript.

GRANTS

This work was supported by the Australian Research Council (ARC) Centre of Excellence in Vision Science (CE0561903) and Centre of Excellence for Integrative Brain Function (CE140100007).

DISCLOSURES

No conflicts of interest, financial or otherwise, are declared by the author(s).

AUTHOR CONTRIBUTIONS

S.L.C. and M.R.I. conception and design of research; S.L.C. and M.R.I. performed experiments; S.L.C contributed unpublished reagents/analytic tools; S.L.C. and M.R.I. analyzed data; S.L.C. and M.R.I. interpreted results of experiments; S.L.C. and M.R.I. prepared figures; S.L.C. and M.R.I. drafted manuscript; S.L.C. and M.R.I. edited and revised manuscript; S.L.C. and M.R.I. approved final version of manuscript.

REFERENCES

Bardy C, Huang JY, Wang C, FitzGibbon T, Dreher B. 'Simplification' of responses of complex cells in cat striate cortex: suppressive surrounds and 'feedback' inactivation. *J Physiol* 574: 731–750, 2006.

Bullier J, Henry GH. Ordinal position and afferent input of neurons in monkey striate cortex. *J Comp Neurol* 193: 913–935, 1979.

Calloway EM. Neural mechanisms for the generation of visual complex cells. *Neuron* 35: 378–380, 2001.

Cavanaugh JR, Bair W, Movshon JA. Nature and interaction of signals from the receptive field center and surround in macaque V1 neurons. *J Neurophysiol* 88: 2530–2546, 2002.

Chance FS, Nelson SB, Abbott LF. Complex cells as cortically amplified simple cells. *Nat Neurosci* 2: 277–282, 1999.

Crowder NA, van Kleef J, Dreher B, Ibbotson MR. Complex cells increase their phase-sensitivity at low contrasts and following adaptation. *J Neurophysiol* 98: 1155–1166, 2007.

Dean AF. The relationship between response amplitude and contrast for cat striate cortical neurones. *J Physiol* 318: 413–427, 1981.

Durand JP, Girard P, Barone P, Bullier J, Nowak LG. Effects of contrast and contrast adaptation on static receptive field featurers in macaque area V1. *J Neurophysiol* 108: 2033–2050, 2012.

Efron B, Tibshirani RJ. *An Introduction to the Bootstrap*. New York: Chapman & Hall, 1993.

El-Shamayleh Y, Kumbhani RD, Dhruv NT, Movshon JA. Visual response properties of V1 neurons projecting to V2 in macaque. *J Neurosci* 33: 16594–16605, 2013.

Felleman DJ, Van Essen DC. Distributed hierarchical processing in the primate cerebral cortex. *Cereb Cortex* 1: 1–47, 1991.

Fitzpatrick D, Lund JS, Blasdel GG. Intrinsic connections of macaque striate cortex: afferent and efferent connections of lamina 4c. *J Neurosci* 5: 3329–3349, 1985.

Foster KH, Gaska JP, Nagler M, Pollen DA. Spatial and temporal frequency selectivity of neurones in visual cortical areas V1 and V2 of the macaque monkey. *J Physiol* 365: 331–363, 1985.

Freeman J, Ziemba CM, Heeger DJ, Simoncelli EP, Movshon JA. A functional and perceptual signature of the second visual area in primates. *Nat Neurosci* 16: 974–981, 2013.

Gilbert CD. Laminar differences in receptive field properties of cells in cat primary visual cortex. *J Physiol* 268: 391–421, 1977.

Girman SV, Sauvé Y, Lund RD. Receptive field properties of single neurons in rat primary visual cortex. *J Neurophysiol* 82: 301–311, 1999.

Green DM, Swets JA. *Signal Detection Theory and Psychophysics*. New York: Wiley, 1966.

Heggelund P. Receptive field organization of simple cells in cat striate cortex. *Exp Brain Res* 42: 89–98, 1981.

Hendrickson AE, Wilson JR, Ogren MP. The neuroanatomical organization of pathways between the dorsal lateral geniculate nucleus and visual cortex in Old World and New World primates. *J Comp Neurol* 182: 123–136, 1978.

Henry CA, Hawken MJ. Stability of simple-complex classification with contrast and extra-classical receptive field modulation in macaque V1. *J Neurophysiol* 109: 1793–1803, 2013.

Henry GH. Receptive field classes of cells in the striate cortex of the cat. *Brain Res* 133: 1–28, 1977.

Hietanen MA, Cloherty SL, van Kleef JP, Wang C, Dreher B, Ibbotson MR. Phase-sensitivity of complex cells in primary visual cortex. *Neuroscience* 237: 19–28, 2013.

Hubel DH, Wiesel TN. Receptive fields, binocular interaction and functional architecture in cats visual cortex. *J Physiol* 160: 106–154, 1962.

Ibbotson MR, Mark RF. Impulse responses distinguish two classes of directional motion-sensitive neurons in the nucleus of the optic tract. *J Neurophysiol* 75: 996–1007, 1996.

Ibbotson MR, Mark RF. Orientation and spatiotemporal tuning of cells in the primary visual cortex of an Australian marsupial, the wallaby *Macropus eugenii*. *J Comp Physiol A* 189: 115–123, 2003.

Ibbotson MR, Price NS, Crowder NA. On the division of cortical cells into simple and complex types: a comparative viewpoint. *J Neurophysiol* 93: 3699–3702, 2005.

Kapadia MK, Westheimer G, Gilbert CD. Dynamics of spatial summation in primary visual cortex of alert monkeys. *Proc Natl Acad Sci USA* 96: 12073–12078, 1999.

Levitt JB, Kiper DC, Movshon JA. Receptive fields and functional architecture of macaque V2. *J Neurophysiol* 71: 2517–2542, 1994.

Lund JS. Anatomical organization of macaque monkey striate visual cortex. *Annu Rev Neurosci* 11: 253–288, 1988.

Lund JS, Hendrickson AE, Ogren MP, Tobin EA. Anatomical organization of primate visual cortex area VII. *J Comp Neurol* 202: 19–45, 1981.

Malpeli JG. Activity of cells in area 17 of the cat in absence of input from layer A of lateral geniculate nucleus. *J Neurophysiol* 49: 595–610, 1983.

Martin KA, Whitteridge D. Form, function and intracortical projections of spiny neurons in the striate visual cortex of the cat. *J Physiol* 353: 463–504, 1984.

Martinez LM, Alonso JM. Construction of complex receptive fields in cat primary visual cortex. *Neuron* 32: 515–525, 2001.

Mata ML, Ringach DL. Spatial overlap of ON and OFF subregions and its relation to response modulation ratio in macaque primary visual cortex. *J Neurophysiol* 93: 919–928, 2005.

Movshon JA, Thompson ID, Tolhurst DJ. Receptive field organization of complex cells in the cat's striate cortex. *J Physiol* 283: 79–99, 1978a.

Movshon JA, Thompson ID, Tolhurst DJ. Spatial summation in the receptive fields of simple cells in the cat's striate cortex. *J Physiol* 283: 53–77, 1978b.

Ohzawa I, Sclar G, Freeman RD. Contrast gain control in the cat visual cortex. *Nature* 298: 266–268, 1982.

Ohzawa I, Sclar G, Freeman RD. Contrast gain control in the cat's visual system. *J Neurophysiol* 54: 651–667, 1985.

Peters A, Payne BR, Budd J. A numerical analysis of the geniculocortical input to striate cortex in the monkey. *Cereb Cortex* 4: 215–229, 1994.

Priebe NJ, Ferster D. Mechanisms of neuronal computation in mammalian visual cortex. *Neuron* 75: 194–208, 2012.

Ringach DL, Shapley RM, Hawken MJ. Orientation selectivity in macaque V1: diversity and laminar dependence. *J Neurosci* 22: 5639–5651, 2002.

Romo PA, Wang C, Zeater N, Solomon SG, Dreher B. Phase sensitivities, excitatory summation fields, and silent suppressive receptive fields of single neurons in the parastriate cortex of the cat. *J Neurophysiol* 106: 1688–1712, 2011.

Rust NC, Schwartz O, Movshon JA, Simoncelli EP. Spatiotemporal elements of macaque V1 receptive fields. *Neuron* 46: 945–956, 2005.

Sceniak MP, Hawken MJ, Shapley R. Contrast-dependent changes in spatial frequency tuning of macaque V1 neurons: effects of a changing receptive field size. *J Neurophysiol* 88: 1363–1373, 2002.

Sceniak MP, Ringach DL, Hawken MJ, Shapley R. Contrast's effect on spatial summation by macaque V1 neurons. *Nat Neurosci* 2: 733–739, 1999.

Sengpiel F, Sen A, Blakemore C. Characteristics of surround inhibition in cat area 17. *Exp Brain Res* 116: 216–228, 1997.

Shushruth S, Ichida JM, Levitt JB, Angelucci A. Comparison of spatial summation properties of neurons in macaque V1 and V2. *J Neurophysiol* 102: 2069–2083, 2009.

Skottun BC, DeValois RL, Grosof DH, Movshon JA, Albrecht DG, Bonds AB. Classifying simple and complex cells on the basis of response modulation. *Vision Res* 31: 1079–1086, 1991.

Smith MA, Majaj NJ, Movshon JA. Dynamics of motion signaling by neurons in macaque area MT. *Nat Neurosci* 8: 220–228, 2005.

Spitzer H, Hochstein S. Complex-cell receptive field models. *Prog Neurobiol* 31: 285–309, 1988.

Tao L, Shelley M, McLaughlin D, Shapley R. An egalitarian network model for the emergence of simple and complex cells in visual cortex. *Proc Natl Acad Sci USA* 101: 366–371, 2004.

Tolhurst DJ, Movshon JA, Dean AF. The statistical reliability of signals in single neurons in cat and monkey visual cortex. *Vision Res* 23: 775–785, 1983.

van Kleef JP, Cloherty SL, Ibbotson MR. Complex cell receptive fields: evidence for a hierarchical mechanism. *J Physiol* 588: 3457–3470, 2010.

Wielaard DJ, Shelley M, McLaughlin D, Shapley R. How simple cells are made in a nonlinear network model of the visual cortex. *J Neurosci* 21: 5203–5211, 2001.

Zhu W, Shelley M, Shapley R. A neuronal network model of primary visual cortex explains spatial frequency selectivity. *J Comput Neurosci* 26: 271–287, 2009.